# Flow simulations with ultra-low Reynolds numbers over rigid and flexible airfoils subject to heaving and flapping motions

D. Antonelli[1,3†], C. Sacco[2], and J. Tamagno[1]

[1] *Cordoba National University, Cordoba, Cordoba, 5000, Argentina*
[2] *Aeronautical University Institute, Cordoba, Cordoba, 5000, Argentina*
[3] *Consejo Nacional de Investigaciones Cientificas y Tecnicas-CONICET, Argentina*

† *Corresponding Author Email*: *dinoantonelli@hotmail.com*

(Received ——; accepted ——)

## ABSTRACT

Numerical simulations of flow patterns at ultra-low Reynolds numbers over rigid and flexible airfoils and the influence of flexibility on main aerodynamic properties, are presented and discussed. Typical unsteady flights like heaving and flapping are, in terms of Reynolds and Strouhal numbers, reduced frequencies and FSI (Fluid Structure Interaction) factor, are valuated. It has been found that for some flexibility levels, the aerodynamic forces and propulsive efficiency are enhanced if compared with a rigid airfoil. The mathematical technical approach used to solve the laminar-incompressible flow equations coupled with structural algorithms, is described.

**Keywords:** Aerodynamic wing sections, CFD, Fluid structure interaction, Unsteady flows, Low Reynolds, Flexible airfoil, Partitioned method, Finite element method.

## NOMENCLATURE

| | |
|---|---|
| $c$ | chord |
| $\mathbf{c}$ | convective velocity |
| $C_D$ | drag coefficient |
| $C_L$ | lift coefficient |
| $C_P$ | power coefficient |
| $C_T$ | thrust coefficient |
| $\bar{c}x$ | generic average coefficient |
| $e$ | structural thickness |
| $E$ | Young modulus |
| $f_h$ | heaving frequency |
| $f_\alpha$ | pitching frequency |
| $h_a$ | heaving amplitude |
| $I$ | Inertial moment |
| $k$ | reducy frequency, iteration |
| $L$ | lift |
| $M$ | Mach number |
| $P$ | input power |
| $p$ | fluid pressure |
| $R_e$ | Reynolds number |
| $U$ | reference velocity |
| $St$ | Strouhal number |
| $t$ | time |
| $T$ | Thrust |
| $\mathbf{u}$ | fluid velocity |
| $\mathbf{u}_s$ | interface structural velocity |
| $\mathbf{u}_f$ | interface fluid velocity |
| $\mathbf{u}_m$ | mesh velocity |
| $\hat{\mathbf{u}}$ | fractionary velocity |
| $w$ | transversal structural displacement |
| $\tilde{\mathbf{w}}$ | interface displacement |
| $\alpha$ | angle of attack |
| $\delta^*$ | flexibility |
| $\delta$ | tip displacement |
| $\Delta t$ | time step |
| $\eta$ | propulsive efficiency |
| $\mu_s$ | structural mass per unit length |
| $\rho_f$ | fluid density |
| $\rho_s$ | structural density |
| $\rho^*$ | density relation |
| $\Sigma$ | FSI intensity factor |
| $\bar{\sigma}$ | fluid stress tensor |
| $\phi_h$ | test elemental function |
| $\chi_\alpha$ | pitching phase |
| $\chi_h$ | heaving phase |
| $\psi_h$ | test elemental function |
| $\omega$ | relaxation Aitkens factor |
| $\Omega$ | analysis domain |

## 1. INTRODUCTION

The importance of ultra-low Reynolds flows lies in technological applications like MAVs (Micro Air Vehicles). They are flying systems with maximum dimensions of $0.15[m]$ that can lead to revolutionary improvements in remote sensing and information gathering capabilities both in military as well in civilian applications Radmanesh et al. (2014). In many cases, an in depth study of phenomena observed in flight is necessary to obtain maximum propulsion with the highest efficiency.

Because of Reynolds number effects, aerodynamic characteristics such as lift, drag and thrust of a flight vehicle change considerably between MAVs and conventional manned air vehicles. In fact, in the nature, birds or insects flap their wings interacting with the surrounding air to generate lift to stay aloft or producing thrust to fly forward. The main powered flights are: heaving and flapping (flights with free stream) and hovering (flight without free stream).

Unsteady aerodynamic mechanisms such as the generation of a leading edge vortex (LEV), wing-wake interaction, and three-dimensional flow features, such as tip vortex-vortex interactions, all significantly affect the aerodynamic force generation. Another remarkable mechanism that the biological flyers seem to be using is the wing flexibility. Studies have been performed to shed light on the interplay between the structural flexibility and the resulting aerodynamic forces.

Much research in this broad area have been made. The most significant that can be named are: Guerrero (2008) carried out unsteady aerodynamic studies at ultra-low Reynolds in $2D$ and $3D$ configurations built using the NACA 0012 wing section; Combes and Daniel (2005) have shown that a variety of insects exhibit anisotropy in their wing structures based on static response tests.

Experimental and numerical studies Kang and Shyy (2012), Kang et al. (2011), Aono et al. (2009) have shown that the chordwise flexibility affects the distribution of the resulting aerodynamic forces in lift and thrust directions. For example, if the plate shape undergoes deformation then the camber of the plate may change, leading to an effective geometry modification, wich combined with the pitching angle the direction of the net force can be adjusted in favor of the thrust generation. Furthermore, for a range of spanwise flexibility, deformed airfoil shapes along the spanwise and the correct direction of the motion, are seen to enhance the thrust of a plunging wing.

Zhu (2007) showed numerically that the thrust and the propulsive efficiencies increased more for a plunging chordwise flexible airfoil in water than immersed in air. Hence it is seen that the flexibility, including the density ratio can be utilized to control resulting aerodynamic forces. However the precise underlying physics of aeroelastic coupling for flapping wings and its applicability to the MAV designs are yet to be understood.

The aerodynamic force generation caused by structural flexibility, is definitely essential to change local behaviors in thrust and propulsive efficiency. Studies like Olivier (2010), Heathcote and Gursul (2005), Chandar and Damodaran (2009), Naderi et al. (2016) analized flexibles and rigid airfoils under sinusoidal flapping motion (or combined pitching and heaving) of flexible insect wings under realistic flight conditions such as forward flight and/or rapid maneuvering.

Ranges of non-dimensional numbers found relevant to unsteady flights of biological ”flappers”, are also considered valid for MAVs. A characteristic one for flapping motions is the Strouhal number $St = 2f_h h_a/U$, where $f_h$ is the frequency and $h_a$ the amplitude of motion. Therefore, the Strouhal number expresses the ratio between the flapping wing velocity and the reference velocity $U$. The reduced frequency given by $k = \pi f_h c/U$ is another parameter that can be interpreted as a measure of unsteadiness comparing the wave length of the flow disturbance to the chord $c$. Then the fundamental aerodynamics parameters are computed by:

$$C_L(t) = \frac{L(t)}{\frac{1}{2}\rho_f U^2 c} \tag{1}$$

where $C_L$ is the lift coefficient. Then the thrust coefficient is:

$$C_T(t) = -C_D(t) = \frac{T(t)}{\frac{1}{2}\rho_f U^2 c} \tag{2}$$

where $T = -D$. and the input power coefficient is:

$$C_P(t) = \frac{P(t)}{\frac{1}{2}\rho_f U^3 c} \tag{3}$$

The thrust efficiency is:

$$\eta = \frac{\bar{T}U}{\bar{P}} = \frac{\bar{ct}}{\bar{cp}} \tag{4}$$

where $\bar{ct}$ and $\bar{cp}$ are the average thrust and power coefficents respectively.[1]

The dimensionless parameters of the flexible flapping wing sections problem are Olivier (2010): flexibility,

$$\delta^* = \frac{\rho_f (f_h h_a)^2 c^3}{EI} \tag{5}$$

wich relates the dynamic pressure with structural stiffness and the FSI intensity factor is defined by,

$$\Sigma = \frac{\rho_f h_a}{\rho_s e} \tag{6}$$

---

[1] The average coefficents are computed by: $\bar{cx} = \frac{1}{\mathbb{T}}\int_t^{t+\mathbb{T}} C_X(t)dt$ where $\mathbb{T}$ is the period of the induced oscillatory motion and $C_X(t)$ can be $P(t)$, $T(t)$, $C_L(t)$, $C_T(t)$, etc.

wich represent the relation between structural inertial forces and aerodynamic pressure. Density relation is:

$$\rho^* = \frac{\rho_s}{\rho_f} \tag{7}$$

2D unsteady flow sinusoidal kinematics are given by the equations:

$$h(t) = h_a sin(2\pi f_h t + \chi_h) \tag{8}$$

$$\alpha(t) = \alpha_a sin(2\pi f_\alpha t + \chi_\alpha) \tag{9}$$

where $\chi_h$ and $\chi_\alpha$ are the phases angles.

## 2. Numerical Method

### 2.1 Fluid Module

The two-dimensional time-dependent Navier-Stokes equations are solved using the finite element method, assuming incompressible-laminar flow which is justified since the Mach number of a MAV flight is $M << 0.3$ and the Reynolds number $R_e < 10000$. To represent the unsteady flow, the Navier-Stokes equations are solved in a fixed inertial reference frame incorporating a moving mesh with velocity $\mathbf{u}_m$ following the Arbitrary Lagrangian Eulerian (ALE) formulation Donea and Huerta (2003). Conservation of mass and momentum in a $\Omega$ analysis domain with boundaries $\Gamma_u \bigcup \Gamma_\sigma$, with $(t_0, t_f)$ time interval of analysis, are described by:

$$\nabla.\mathbf{u} = 0 \tag{10}$$

$$\frac{\partial(\mathbf{u})}{\partial t} + (\mathbf{c}.\nabla)\mathbf{u} + \frac{1}{\rho_f}\nabla p - \nu\nabla^2\mathbf{u} - \mathbf{f}_e = \mathbf{0} \tag{11}$$

The $\mathbf{u}$ is the two-dimensional flow velocity vector, $\rho_f$ the constant density, $\nu$ the kinematic viscosity, $p$ the pressure, $\mathbf{f}_e$ the external forces and $\mathbf{c} = \mathbf{u} - \mathbf{u}_m$ is the convective velocity that represent the difference between fluid velocity and mesh velocity. In the present work, the algorithm of mesh movement is based in operations of optimal smoothing, developed by Canann et al. (1998).

The equations previously presented can not be solved by a numerical standard form because incompressibility gives raise to a flow field restriction. There are several algorithms to deal with this difficulty and the *Fractional Step* method used here is one of them. The method meets the LBB condition Babuska (1971) through the use of same order of approximation for velocity and pressure. To apply the Fractional Step algorithm the momentum equation 11 without mesh movement $\mathbf{u}_m = 0$ is divided in two parts,

$$\hat{\mathbf{u}}^{n+1} = \mathbf{u}^n + \delta t \left[\mathbf{u}^{n+\theta}.\nabla\mathbf{u}^{n+\theta} + \gamma\frac{1}{\rho_f}\nabla p^n - \nu\nabla^n\mathbf{u}^{n+\theta} + \mathbf{f}^{n+\theta}\right] \tag{12}$$

$$\mathbf{u}^{n+1} = \hat{\mathbf{u}}^{n+1} - \frac{\delta t}{\rho_f}(\nabla p^{n+1} - \gamma\nabla p^n) \tag{13}$$

In the Eq. 12 the fractionary velocity $\hat{\mathbf{u}}$ is introduced and used in Eq. 13. If the divergence of Eq. 13 is taken and the continuity equation is applied, results:

$$\nabla^2(p^{n+1} - \gamma p^n) = \frac{\rho_f}{\delta t}\nabla.\hat{\mathbf{u}}^{n+1} \tag{14}$$

Through this equation the pressure is calculated. In addition, $\gamma$ is a numerical parameter such that its values of interest are 0 and 1. The $\theta$ parameter determine the kind of temporal approximation.

Then the Finite Element Method is used to discretize the govern equations and it provides an appropriate resolution procedure Lohner (2001). The resultant scheme is of first order ($\gamma = 0$) and the temporal discretization ($\theta = 0$) results in Euler forward. The test functions $(\psi_h, \phi_h) \in \Psi_h \times \Phi_h$ are used such as:

$$\frac{1}{\delta t}(\hat{\mathbf{u}}_h^{n+1}, \psi_h) = \frac{1}{\delta t}(\mathbf{u}_h^n, \psi_h) - (\mathbf{u}_h^n.\nabla\mathbf{u}_h^n, \psi_h) - \nu(\nabla\mathbf{u}_h^n, \nabla\psi_h) - (\mathbf{f}_e^n, \psi_h) \tag{15}$$

$$(\nabla p_h^{n+1}, \nabla\phi_h) = \frac{\rho_f}{\delta t}\left[(\hat{\mathbf{u}}_h^{n+1} - \mathbf{u}_h^n, \nabla\phi_h) - (\nabla\mathbf{u}_h^n, \phi_h)\right] \tag{16}$$

$$(\mathbf{u}_h^{n+1}, \psi_h) = (\hat{\mathbf{u}}_h^n, \psi_h) - \frac{\delta t}{\rho_f}(\nabla p_h^{n+1}, \phi_h) \tag{17}$$

where subindex $h$ means it is applied on one element. The last equations system is semi-implicit because Eqs. 15 and 17 are explicit (lumped mass matrix) and Eq. 16 for the pressure computation is implicit [2].

The discretization of convective terms yields numerical instabilities, therefore stabilization methods must be used. In this work the *Orthogonal Subgrid Scale* (OSS) algorithm is applied Codina (2000b), Codina (2000a), Principe and Codina

---

[2] The notation used in the equations means: $(\mathbf{a}, \mathbf{b}) = \int \mathbf{a}.\mathbf{b}d\Omega$

(2009). The expresion for the convective stabilization term $STB_u$ is:

$$STB_u = \tau_1(\mathbf{u}_h^n.\nabla\mathbf{u}_h^n - \pi_h^n, \mathbf{u}_h^n\nabla\psi_h) \tag{18}$$

where $\pi_h^n$ is the convective term projection and it is defined in Eq. 23. This equation add to momentum Eq. 15 and it is evaluated in $t^n$, therefore it remains explicit.

The term stabilization of pressure $STB_p$ to be added to the Eq. 16 is:

$$STB_p = -(\tau_2(\nabla p^n - \xi_h^n), \nabla\phi_h) \tag{19}$$

where $\xi_h^n$ is the gradient pressure term projection and it is defined in Eq. 24. In addition, it is evaluated in $t^n$, therefore it remains explicit.

The final complete stabilized scheme with mesh movement $\mathbf{u}_m$ is obtained:

$$\begin{aligned}\frac{1}{\delta t}(\hat{\mathbf{u}}_h^{n+1}, \psi_h) = {} & \frac{1}{\delta t}(\mathbf{u}_h^n, \psi_h) - (\mathbf{c}_h^n \cdot \nabla\mathbf{u}_h^n, \psi_h) \\ & - \nu(\nabla\mathbf{u}_h^n, \nabla\psi_h) - (\mathbf{f}_e^n, \psi_h) \\ & - (\tau_1(\mathbf{c}_h^n \cdot \nabla\mathbf{u}_h^n - \pi_h^n), \nabla\mathbf{c}_h^n \cdot \nabla\psi_h)\end{aligned} \tag{20}$$

$$\begin{aligned}(\nabla p_h^{n+1}, \nabla\phi_h) = {} & \\ & \frac{\rho_f}{\delta t + \tau_2}\left[(\hat{\mathbf{u}}_h^{n+1} - \mathbf{u}_h^n, \nabla\phi_h) - (\nabla\mathbf{u}_h^n, \phi_h)\right] \\ & + \frac{\tau_2}{\delta t + \tau_2}(\nabla\xi_h^n, \nabla\phi_h)\end{aligned} \tag{21}$$

$$(\mathbf{u}_h^{n+1}, \psi_h) = (\hat{\mathbf{u}}_h^n, \psi_h) - \frac{\delta t}{\rho_f}(\nabla p_h^{n+1}, \phi_h) \tag{22}$$

$$(\pi_h^n, \widetilde{\psi}_h) = (\mathbf{c}_h^n.\nabla\mathbf{u}_h^n, \widetilde{\psi}_h) \tag{23}$$

$$(\xi_h^n, \widetilde{\psi}_h) = (\nabla p_h^n, \widetilde{\psi}_h) \tag{24}$$

where $\widetilde{\psi}_h \in \widetilde{\Psi}_h$ and $\tau_1$, $\tau_2$ are stabilization coefficents. The system of equations of Eqs. 20, 22, 23, 24 are solved in explicit form with lumped mass matrix and the system resultant of Eq. 21 is solve in explicit form through of conjugate gradients with diagonal pre-conditioner.

It is noted that the formulation of the scheme isn't in the ALE framework. To account the mesh velocity it is necessary to introduce the convective velocity **c** in convective and stabilization terms.

Finally the boundary conditions in viscous tensor and velocity are:

- Imposed velocity: $\mathbf{u} = \mathbf{u_c}$
- No slip: $\mathbf{u} = \mathbf{0}$
- No traction: $\mathbf{n}.\bar{\sigma}.\mathbf{n} = 0$

where $\bar{\sigma}$ is the fluid stress tensor and **n** a normal surface versor.

### 2.2 Structural Module

The govern equation of the structural model is:

$$\frac{\partial^2}{\partial x^2}\left(EI\frac{\partial w^2}{\partial x^2}\right) = -\mu_s\frac{\partial w^2}{\partial t^2} + q(x) \tag{25}$$

where $w$ is the transverse displacement, $\mu_s$ is the mass per unit length, $E$ Young's modulus, $I$ inertial moment and $q(x)$ a distributed transverse load.

Computations done for a flexible airfoil composed of a rigid teardrop and elastic flat plate at higher Reynolds number and for various motion frequencies, Kang et al. (2011) showed that a linear Euler-Bernoulli beam is sufficient for the analysis of the fluid-structure interaction.

The Euler-Bernoulli beam model has been incorporated to solve Eq. 25 using a finite element (FE) representation. The structural damping is not considered in this study and two degree of freedom, i.e. displacement and bending, are allowed at each node. The FE solution approach Cook et al. (2001), Wright and Cooper (2007) is given by the following steps:

- Determine the dynamic properties of each element in the form of element stiffness and mass matrices. In order to write the strain energy and the kinetic energy terms for the element, the variation of displacement within the element will need to be expressed as a function of the nodal displacements. It is assumed that the variation of the transverse displacement along the beam elements can be expressed as a cubic polynomial.
- Assemble all the elements to form global mass and stiffness matrices from which modes and responses may be determined. The assembly process satisfies exact compatibility of displacements/rotations between elements. The advantages of the finite element method are that more elements may be used in regions where the displacement and/or stress is expected to vary more rapidly and that more complex geometries and problems may be handled. The general equation to solve is:

  $$\mathbf{M}_r\ddot{\mathbf{r}} + \mathbf{K_r}\mathbf{r} = \mathbf{R} \tag{26}$$

  where $\mathbf{M}_r$ is the global mass matrix, $\mathbf{r}$ is the displacements vector, $\mathbf{K_r}$ is the global stiffness matrix and **R** is the external forces vector.

- Solve the general eq. 26 via damped Newmark time integration scheme.

### 2.3 Coupling Strategy

The fluid-structure interaction is based on a time-domain partitioned solution process, in which the partial differential equations governing the fluid and the structure are solved independently and spatially coupled, through the interface between the fluid and the structure Degroote (2010). At each time step the fluid **F** and structural **S** solvers are called one after the other, until sufficient convergence on the displacements on the shared boundary surface are reached in an inner-iteration before advancing to the next time step.

Since both fluid and structure have been modeled with continuous theory, the treatment of the fluid-solid interface makes no exception. Only the mass conservation and the momentum conservation equations are considered as the other physics principles are not required to describe elastic solid and nearly incompressible flows. Therefore, the momentum and mass conservation at the FSI interface yields the following conditions Olivier (2010):

$$\begin{aligned}&\mathbf{u}_s = \mathbf{u}_f\\ &\bar{\sigma}_f \cdot \mathbf{n} = \bar{\sigma}_s \cdot \mathbf{n}\end{aligned}\tag{27}$$

which means that the fluid ($f$ subindex) and structural ($s$ subindex) velocities and normal loads, are equals in the interface. These conditions are implemented in the code following the method presented in Maza et al. (2012).

In this work, the strong coupling block Gauss-Seidel partitioned method with relaxation Vazquez (2007), Kuttler and Wall (2008) has been implemented. Starting from known values of fluid structure and mesh in time $t_n$, a scheme of the coupling algorithm is presented in Fig. 1.

## 3. VERIFICATION OF NUMERICAL CODE

### 3.1 Verification of Baseline Solvers

As a verification case of the fluid solver, a rigid NACA 0012 airfoil in flapping motion is analyzed. The following parameters are considered: pitching and heaving frequencies $f_\alpha = f_h = 0.225Hz$, reducy frequency $k = 0.7096$, maximum heaving amplitude $h_a = 1$, phase angle $\chi_\alpha = 90°$, Strouhal number $St = 0.45$ and the variable parameter is the pitching amplitude $\alpha_a$.

In the Table 1 a comparison of maximum lift coefficient $C_{Lm}$ and average thrust coefficient $\bar{ct}$ is presented. It can be concluded that the results obtained in this work compare well with those given by Pedro et al. (2003) and Guerrero (2008).

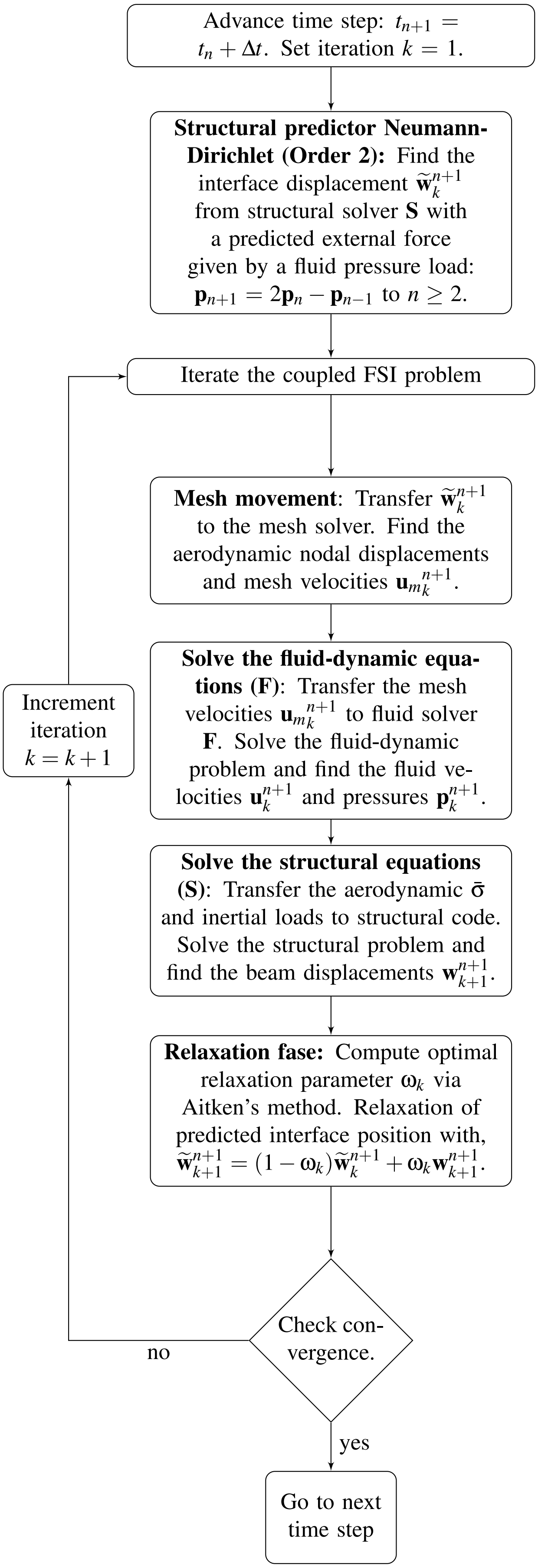

**Fig. 1.** Chart of fluid-structure interaction coupling algorithm.

**Table 1 Comparison of average thrust coefficient $\bar{ct}$ and maximum lift coefficient $C_{Lm}$ in flapping motion for rigid NACA 0012.**

| | Pedro et al. | | Guerrero | | P. Work | |
|---|---|---|---|---|---|---|
| $\alpha_a$ | $\bar{ct}$ | $C_{Lm}$ | $\bar{ct}$ | $C_{Lm}$ | $\bar{ct}$ | $C_{Lm}$ |
| 5° | 0.43 | 8.33 | 0.42 | 8.08 | 0.43 | 8.21 |
| 10° | 0.65 | 7.48 | 0.66 | 7.17 | 0.66 | 7.24 |
| 15° | 0.82 | 6.63 | 0.84 | 6.54 | 0.82 | 6.39 |
| 20° | 0.93 | 5.82 | 0.94 | 6.11 | 1.00 | 5.51 |
| 25° | 1.00 | 5.06 | 0.96 | 5.61 | 1.09 | 4.99 |

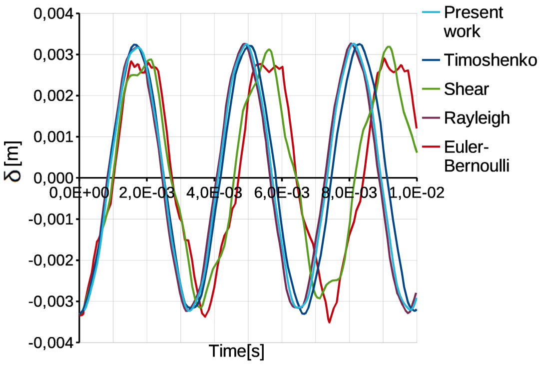

**Fig. 2.** Comparison of tip displacement of beam with prefixed displacement.

As a case for validating the solid module, a vibrating cantilever beam model with prefixed displacement is analyzed. This problem were solved by Han et al. (1999) with four differents theoretical models (Euler-Bernoulli, Shear, Rayleigh and Timoshenko), through the method of eigenfunction expansion.

The beam properties are: length $L = 1m$, tubular section: internal ratius $r_i = 0.15m$, external ratius $r_e = 0.16m$, section area $A = 0.0097389m^2$, area inertial moment $I = 0.0001171m^4$ and density $\rho_s = 7830kg/m^3$. Twenty finite unidimensional elements along the beam were used. The function of initial transversal displacement $w(x,0)$ is:

$$w(x,0) = (1.667x^3 - 5x^2)10^{-3} \tag{28}$$

where $x$ is the coordinate along beam.

The tip displacements of the beam due to differents methods are presented in the Fig. 2. The agreement with the analytic results can be observed.

## 3.2 Verification of FSI Solver

The present FSI solver is verified with a slender flexible structure fixed at the downstream end of a bluff body. The body generates vorticity wich induces oscillations in flexible structure. This problem was proposed originally by Wall and Ramm (1998). The domain and boundary conditions are presented in Fig. 3. The material properties of the structure are density $\rho_s = 0.1Kg/m^3$ and Young modulus $E = 2.5e6$. The flow properties are density $\rho_f = 1.18e-3Kg/m^3$, dynamic viscosity $\mu = 1.82e-4Kg/m.s$ and free stream velocity $U = 51.3m/s$. The Reynolds number is $R_e = 333$ with the side length of the square rigid body used like caracteristic length $L_b = 1m$. The fluid-structure interaction is strong with a the density relation of $\rho^* = 84.74$.

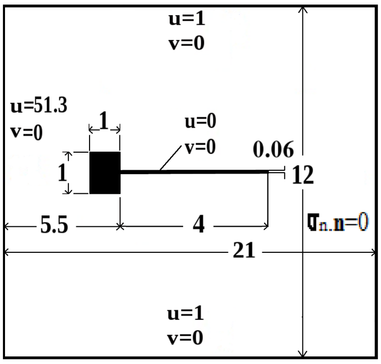

**Fig. 3.** Problem FSI domain specifications (out of scale).

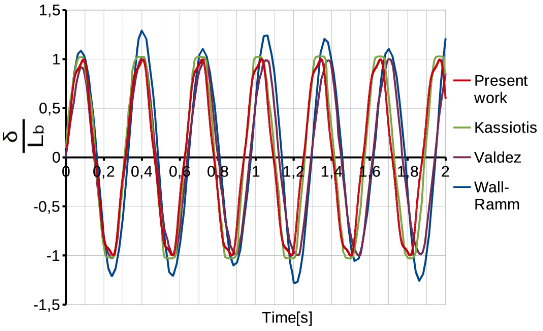

**Fig. 4.** Comparison of tip displacement of flexible structure fixed at bluff body.

**Table 2 Comparison for FSI problem**

| | P. Work | Kassiotis | Valdez | Wall |
|---|---|---|---|---|
| $f_{fs}$[1/s] | 3.186 | 3.175 | 3.125 | 3.071 |
| $err_f$[%] | - | 0.352 | 1.940 | 3.700 |
| $\delta$[m] | 0.998 | 1.031 | 0.997 | 1.328 |
| $err_a$[%] | - | 3.200 | 0.10 | 24.80 |

The fluid-dynamic mesh domain has 24745 elements and the structural mesh has 40 unidimensional elements. The Fig. 4, shows the periodic states obtained by different authors Wall and Ramm (1998), Kassiotis et al. (2011), Vazquez (2007) in comparison with the present work. In this work, the periodic state is assumed when the difference between maximums amplitudes is lower than 0.05. A close agreements are observed between the present

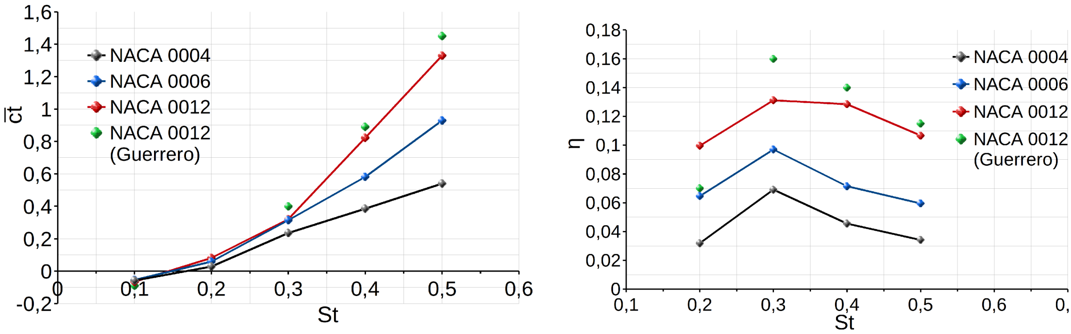

**Fig. 5.** Average thrust coefficient $\bar{ct}$ and propulsive efficiency η for rigid airfoils in heaving motion (NACA 0004, 0006 and 0012).

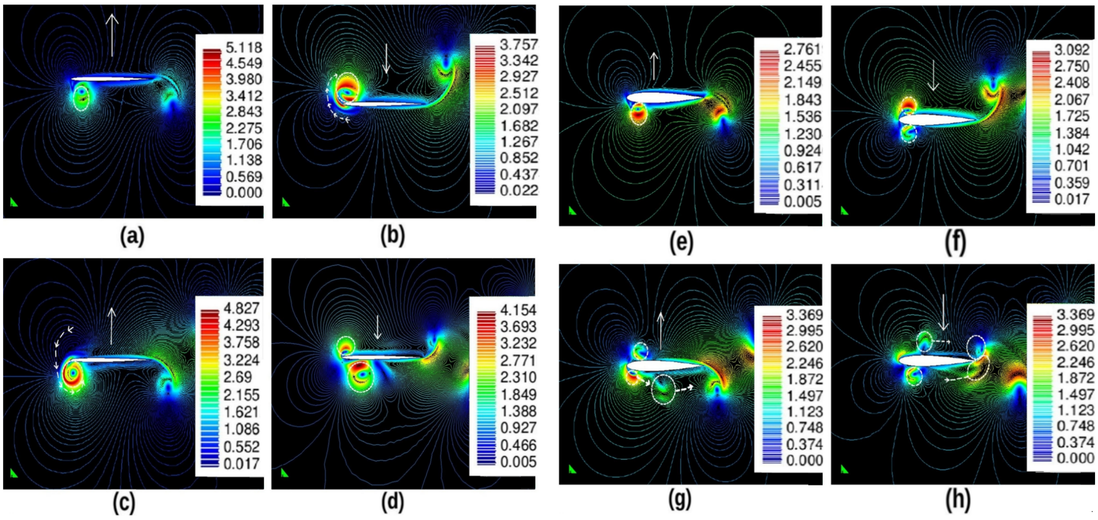

**Fig. 6.** Velocity contours for rigid NACA 0004 (a,b,c,d) and NACA 0012 (e,f,g,h) in heaving motion ($St = 0.3$).

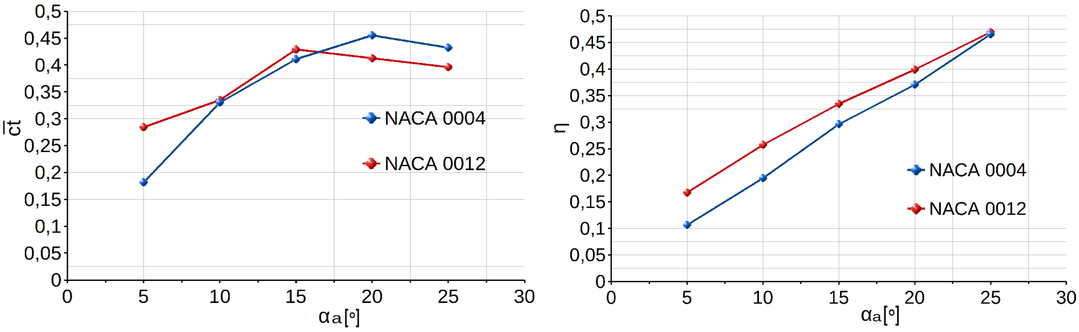

**Fig. 7.** Average thrust coefficient $\bar{ct}$ and propulsive efficiency η as function of $\alpha_a$ in flapping motion of rigid airfoils (NACA 0004 and 0012).

computed results and the numerical values of the authors, mentioned above.

To complete the analysis in Table 2 a comparison between response frequencies $f_{fs}$ and maximum tip displacements $\delta$ with respective errors are listed [3].

## 4. NUMERICAL RESULTS

The fundamental parameter of unsteady analysis is the Strouhal number, defined as $St = 2fh_a/U$. Taylor et al. (2003) and Triantafyllou et al. (1993) performed a study of wing frequencies and amplitudes, and cruise speeds across a range of birds, insects, fishes and cetaceans, to determine Strouhal numbers in "cruising" flight. They found 75% of the 42 species considered fall within a narrow range of $0.19 < St < 0.41$ Guerrero (2008). Therefore, a similar range of Strouhal numbers in this work has been selected.

### 4.1 Heaving motion of rigid airfoils

The first analysis is a heaving motion with kinematic described by Eq. 8. The analysis is applied to NACAs four digits (0004, 0006 and 0012) symmetrical rigid airfoils. The kinematics parameters are: heaving frequency $f_h = 1Hz$ and a variable Strouhal number throughout the heaving amplitude $0.1 < h_a < 0.5$ and $R_e = 1100$. The average thrust coefficient $\bar{ct}$ and propulsive efficiency $\eta = \bar{ct}/\bar{cp}$ in terms of the Strouhal number are presented in Fig. 5. Note that the numerical results obtained by Guerrero (2008) are added. It can be seen in Fig. 5 that thrust and propulsive efficiency increase with airfoil thickness.

Comparisons between velocity contours of NACA 0004 and NACA 0012 airfoils at differents times Fig. 6, helps to understeand the simulation results shown in Fig. 5. Times in Figs. 6 (a) and (e) is $t = 0.45s$, (b) and (f) $t = 0.86s$, (c) and (g) $t = 1.29s$ and (d) and (h) $t = 1.64s$. The formation of leading edge vortices (LEV) and its convection toward the wake, can be detected. With NACA 0004 the LEV remains longer time at the nose that it does with NACA 0012, and the low pressure created there delays convection of th vortex toward the wake and therefore affecting the propulsive and its efficiency.

### 4.2 Flapping motion of rigid airfoils

The second analysis is the flapping motion. The name flapping is applicable to a combined motion of heaving and pitching, consequently the kinematics relations given by sinusoidal Eqs. 8 and 9 are simultaneously applied.

In Fig. 7 are shown average thrust coefficients $\bar{ct}$ and propulsive efficiencies $\eta$ applicable to NACA symmetric rigid airfoils 0004 and 0012, as function of the pitching angle $5° < \alpha_a < 25°$ with $f_\alpha = f_h = 0.3$, $h_a = 0.5m$, $\chi_\alpha = \pi/2$ and $St = 0.3$. The thrust and efficiency are positives in all cases obtained and greater than obtained in heaving motion for rigid airfoils. Both geometries show a similar $\bar{ct}$ curve although NACA 0012 is somewhat more efficient than NACA 0004. In Fig. 8 are shown average thrust coefficients $\bar{ct}$ and propulsive efficiencies $\eta$ applicable to NACA symmetric rigid airfoils 0004 and 0012, as function of the heaving amplitude $0.025 < h_a < 0.5$ $(0.05 < St < 1)$ with $f_h = f_\alpha = 1$, $\alpha_a = 15°$ and $\chi_\alpha = \pi/2$. The $\bar{ct}$ coefficient always increases with the heaving amplitude. The efficiency shows a tendency to increase up to $h_a = 0.1$ $(St = 0.3)$ and then decreases for larger amplitudes.

### 4.3 Heaving motion of flexible airfoils

An analysis of the influence of flexibility $\delta^*$ (Eq. 5) and fluid-structure interaction intensity factor $\Sigma$ in two symmetric airfoils NACA 0012 and NACA 0004 in heaving motion, is performed. The same sinusoidal kinematic and parameters of rigid airfoils are used. The Strouhal number is fixed to $St = 0.3$ (maximum efficiency obtained in rigid airfoils). The variable parameters through Young modulus $E$ are $8.707e-6 < \delta^* < 8,707e-3$ and through structural density $\rho_s$, $0.217 < \Sigma < 1.783$.

The average traction coefficient $\bar{ct}$ and the efficiency $\eta$ are presented in Figs. 9 (NACA 0012) and 10 (NACA 0004). It can be seen the same behavior in both airfoils, although little higher values for NACA 0004. When the structural flexibility is lower than $\delta^* > 1e-3$, the coefficients are almost equals to the rigid airfoils (the deformation is very small). When the flexibility $\delta^* > 1e-3$, $\bar{ct}$ increases to a maximum value and then decreases. When the FSI intensity factor $\Sigma$ is diminished (structural density $\rho_s$ is increased), $\bar{ct}$ is increased. Note that efficiency $\eta$ is dependent of $\bar{cp}$, that it presents a high decrease with $\delta^*$.

As in the analysis of rigid airfoils, a comparison at different times of velocity contours between flexibles NACA 0004 and NACA 0012 (Fig. 11) helps to understand the results of the simulations. The case selected is $\delta^* = 2,64e-003$ and $\Sigma = 0,26168$. Times in Fig. 11 are the same used with rigid airfoils. These are (a) and (e) is $t = 0.45s$; (b) and (f) $t = 0.86s$; (c) and (g) $t = 1.29s$ and (d) and (h) $t = 1.64s$. In both airfoils the leading edge vortexes are convected faster than rigid airfoils. A low pressure region is generated in the lower surface during the upstroke and in the upper surface during the downstroke. In addition, the flexion of airfoil increases the low presion and improves the convec-

---

[3] The error was calculated like $err_f = \frac{f_p - f_r}{f_r}$ where $f_p$ is the present work frequency and $f_r$ the referenced frequency. To the max. tip displacement errors the same form is applied.

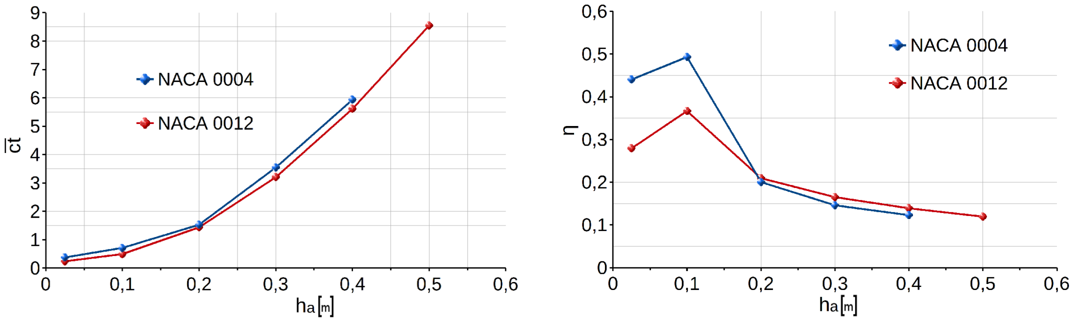

**Fig. 8.** Average thrust coefficient $\bar{ct}$ and propulsive efficiency η as function of $h_a$ in flapping motion of rigid airfoils (NACA 0004 and 0012).

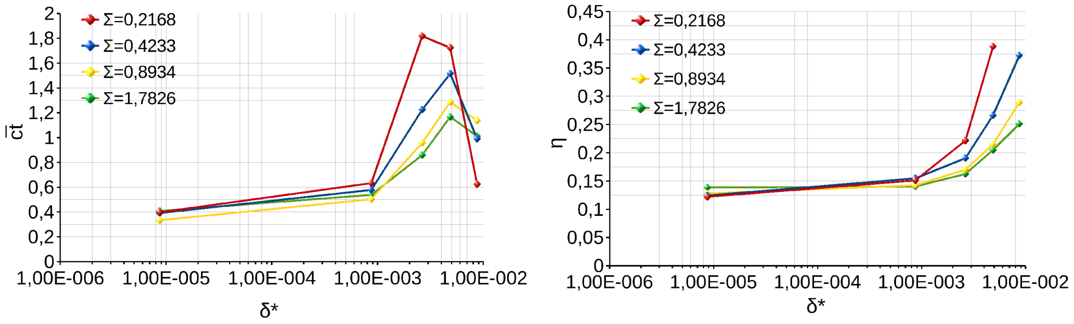

**Fig. 9.** Thrust coefficient $\bar{ct}$ and propulsive efficiency η in heaving motion for flexible NACA 0012.

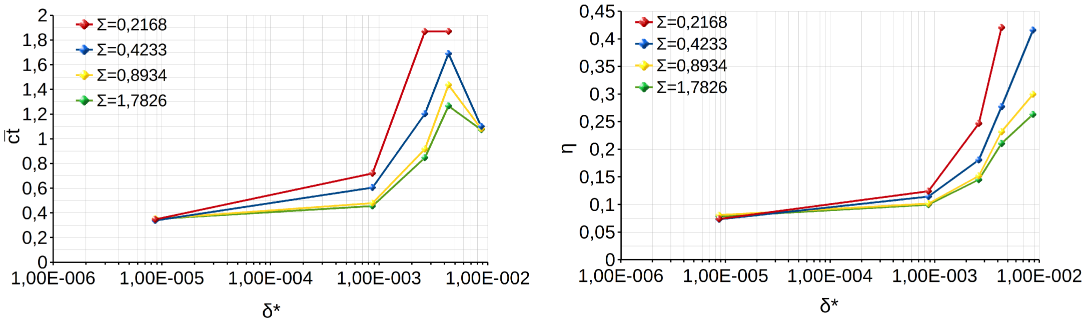

**Fig. 10.** Thrust coefficient $\bar{ct}$ and propulsive efficiency η in heaving motion for flexible NACA 0004.

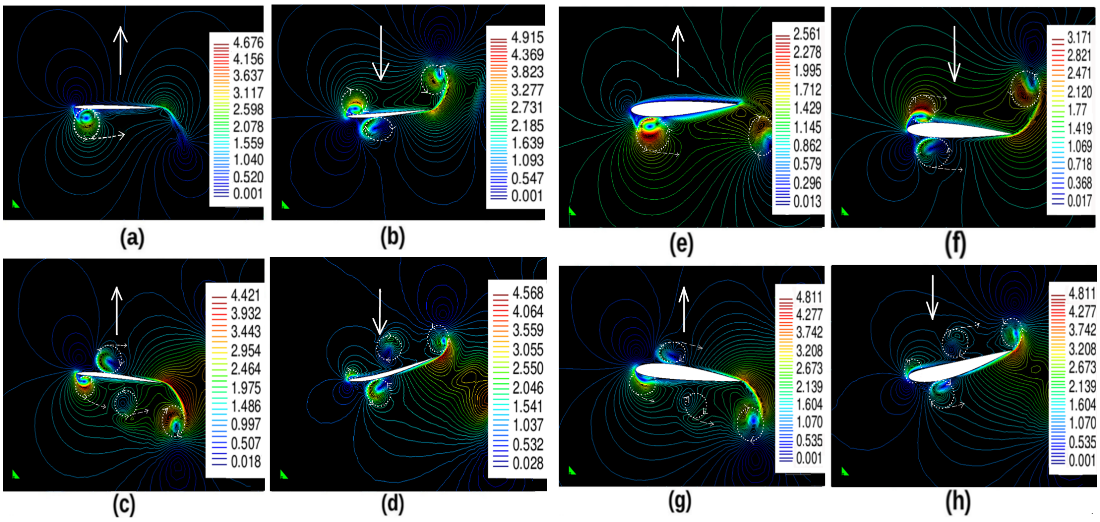

(a) (b) (e) (f)

(c) (d) (g) (h)

**Fig. 11.** Velocity contours for flexible NACA 0004 (a,b,c,d) and NACA 0012 (e,f,g,h) in heaving.

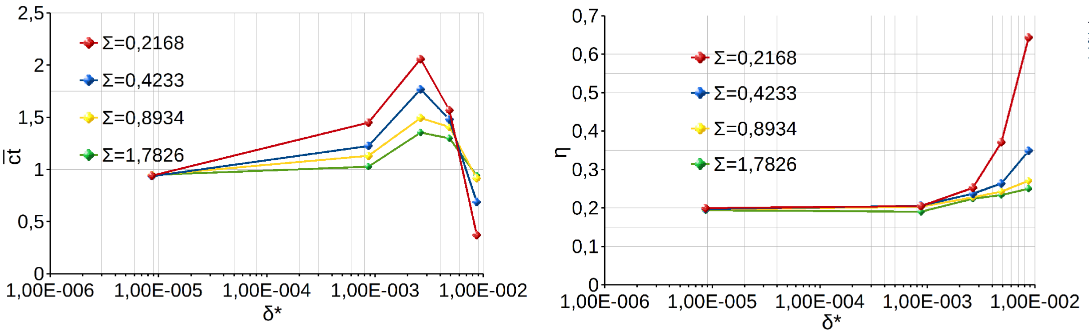

**Fig. 12.** Thrust coefficient $\bar{ct}$ and propulsive efficiency η in flapping motion for flexible NACA 0012.

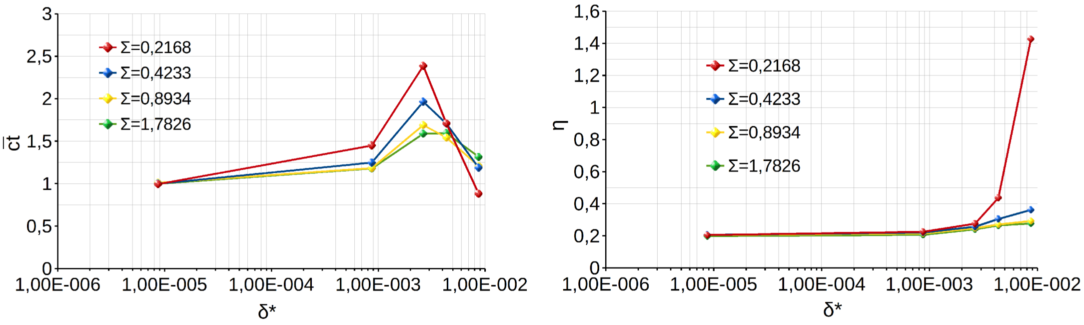

**Fig. 13.** Thrust coefficient $\bar{ct}$ and propulsive efficiency η in flapping motion for flexible NACA 0004.

tion of LEV toward the trailing edge and its coupling with the wake. The consequence is a increase in $\bar{c}t$ and $\eta$ like the results are showing.

## 4.4 Flapping motion of flexible airfoils

### 4.41 Sinusoidal kinematic

The next analysis applies to flapping motion on flexible airfoils. The kinematics are sinusoidal and the parameters of motion are $St = 0.3$ ($h_a = 0.15$), $R_e = 1100$, $f_h = f_\alpha = 1$, $\alpha_a = 10°$ and $\chi_\alpha = \pi/2$. It is observed in Figs. 12 and 13 that in both airfoils, $\bar{c}t$ has increased with respect the value obtained in heaving motion. Maximum $\bar{c}t$ from flapping are limited to the interval of flexibility $1e-3 < \delta^* < 1e-2$, and this interval is the same for maximum $\bar{c}t$ produced in heaving motion.

Note that greater $\bar{c}t$ values are for minimum $\Sigma$ or higher $\rho_s$ values. If the efficiency $\eta$ is compared with the results obtained in flexible airfoils in heaving motion, the difference found between maximums values of $\bar{c}t$ are not big, it can be concluded that in certain cases the structural flexibility can replace rotations mechanism in MAVs, saving some weight.

### 4.42 Alternative kinematic

A third analysis of flexible airfoils in flapping motion with an alternative kinematic is performed. This kinematics is characterized by Eqs. 29 and 30:

$$h(t) = \frac{h_a}{sin^{-1}(0.8)}\, sin^{-1}\left(0.8\, sin(2\pi f_h t)\right) \tag{29}$$

$$\alpha(t) = \frac{\alpha_a}{tanh^{-1}(3)}\, tanh^{-1}\left(3\, sin(2\pi f_\alpha t + \chi_\alpha)\right) \tag{30}$$

The model takes the wing kinematic used in the Robofly model of Dickinson et al. (2004) and Bos et al. (2007). Based on observation of true insect flights, it was accepted that the wing maintains a constant velocity and angle of attack during most of the stroke, with a relatively strong linear and angular acceleration during stroke reversal. This results with typical "sawtooth" displacement and "trapezoidal" angle of attack pattern of the Robofly kinematic model, are illustrated in Fig. 14. The parameters of kinematic are the same used in sinusoidal kinematic, $St = 0.3$ ($h_a = 0.15$), $R_e = 1100$, $f_h = f_\alpha = 1$, $\alpha_a = 10°$ and $\chi_\alpha = \pi/2$.

In the Figs. 15 and 16 the average thrust $\bar{c}t$ and efficiency $\eta$ are presented. In both airfoils is detected an increase in the thrust respect to the sinusoidal kinematic, and the maximum values are between $1e-4 < \delta^* < 1e-3$. The greater $\bar{c}t$ values (minimum $\Sigma$) are given by the NACA 0004 airfoil. In the alternative kinematic, the angle of attack remains in its position of maximum amplitude for longer time, because of its "trapezoidal" pattern (Fig. 14). This implies that vortices generated at the trailing edge (TEV) are more intense, as a results high speed there is in the wake. Therefore, in the leading edge exist a high suction during more time in comparison with sinusoidal kinematic wich allows better convection of generated (LEV). Since both edges in NACA 0004 are sharper than in NACA 0012, the convection is even more intense.

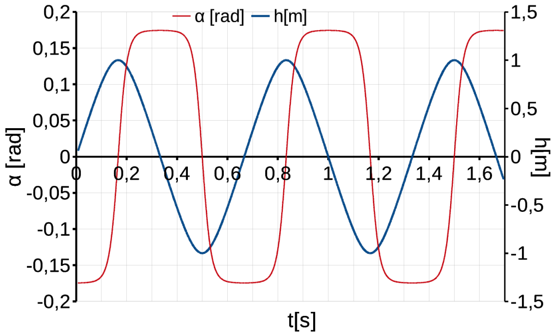

**Fig. 14.** Alternative kinematic.

The propulsive efficiency presents a different behavior respect to the sinusoidal kinematics and the maximums values are between $1e-4 < \delta^* < 5e-3$ , however it depends of average power coefficient $\bar{c}p$.

## 5. CONCLUSIONS

In heaving motion studies, rigid and flexible symmetrical wing sections are considered. Average thrust coefficients and propulsive efficiencies for selected motion frequencies are numerically simulated, and the results plotted in terms of a Strouhal number determined using the heaving amplitude. As a help to better understand the simulation results, velocity contour pictures allowing comparison between wing sections at prescribed identical times, are built and shown. Based on these pictures, generation and displacement of vortexes as the wing section executes the heaving motion are described, and justifications about why an airfoil has better performances than other one when executing such motion, are given. Studies related to the influence of flexibility and FSI intensity factor on thrust coefficients and propulsive efficiencies in heaving motions, are made. From comparisons with rigid data it is concluded that for some flexibility values, improvements are feasible.

Combinations of pitching and heaving motions (flapping) for rigid and flexible wing sections, have also been simulated. Like in rigid airfoils, the maximum pitch angle and vertical displacement am-

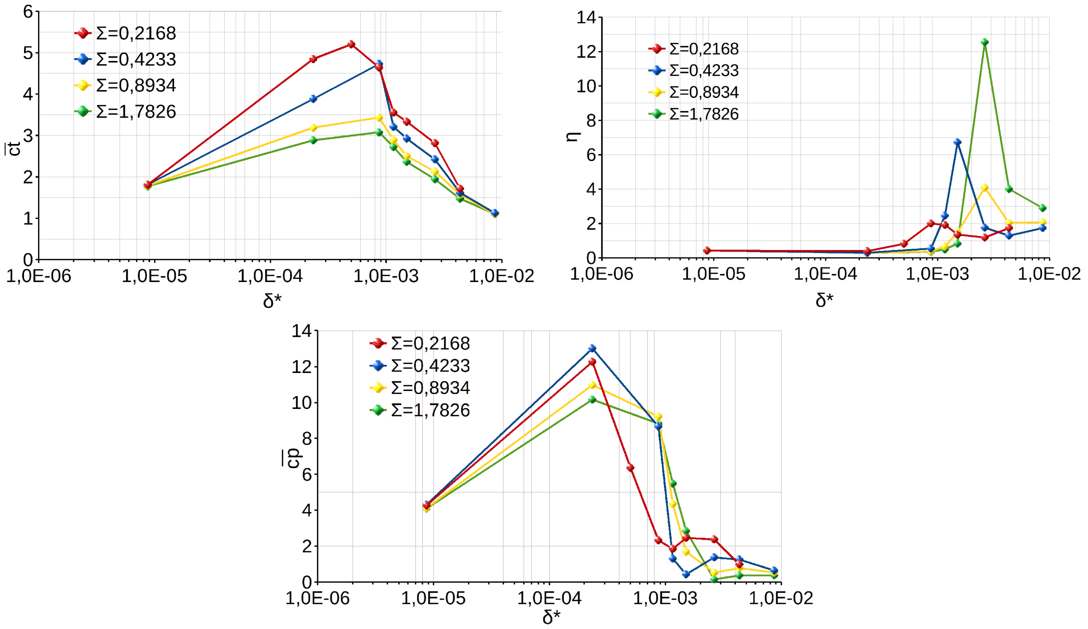

**Fig. 15.** Average $\bar{ct}$, $\bar{cp}$ and η coefficients in alternative flapping kinematic (NACA 0004).

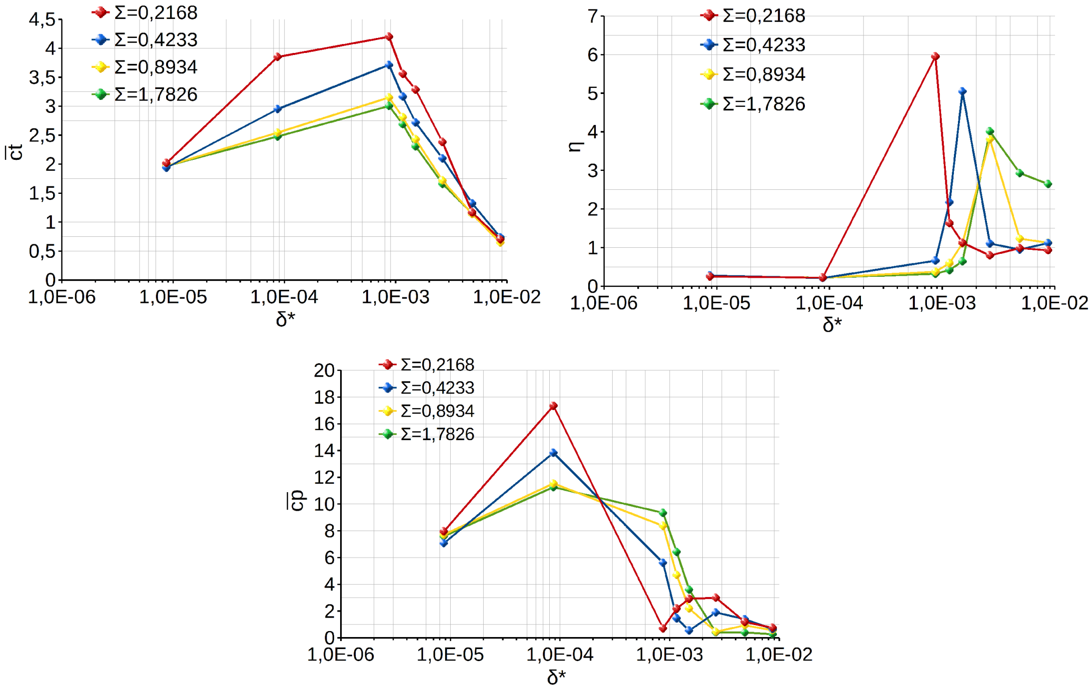

**Fig. 16.** Average $\bar{ct}$, $\bar{cp}$ and η coefficients in alternative flapping kinematic (NACA 0012).

plitudes are taken as plotting variables. It is found that for given pitch angles a maximum propulsion value exist, and this maximum increases when the heaving amplitude of the flapping motion, is also increased. With flexible airfoils, a comparison between two flapping kinematics is performed. In both kinematics, the influence of flexibility and FSI intensity factor on propulsion and its efficiency are studied. Between the sinusoidal kinematic and heaving motion, a similar behavior is found. Therefore, the possibility exist of somehow using wing flexibility (passive pitching) to replace pitching motion hardware in MAV applications and so, the weight can be reduced.

The Finite Element software here used can in run time, build moving grids needed to perform numerical simulations of unsteady motions like heaving and flapping with rigid as well as with flexible 2D wing sections. For dealing with flexible wing sections, an appropriate structural module and algorithms to compute fluid-structure interactions (FSI), are implemented. In addition, and to handle complex geometries, more elements are created in regions where it is expected that displacements and/or strains vary rapidly.

## ACKNOWLEDGMENTS

To CONICET and Aeronautical departament of UNC for the financial and facilities support to this research.

## REFERENCES

Aono, H., S. Chimakurthi, C. Cesnik, H. Liu, and W. Shyy (2009). Computational modeling of spanwise effects on flapping wing aerodynamics. *AIAA 1270.*

Babuska, I. (1971). Error bounds for finite element method. *Numer. Math. 16*, 322–333.

Bos, F., D. Lentink, B. van Oudheusden, and H. Bijl (2007). Numerical study of kinematic wing models of hovering insect flight. *45th AIAA Aerospace Sciences Meeting and Exhibit 482.*

Canann, S. A., J. R. Tristano, and M. L. Staten (1998). An approach to combined laplacian and optimization-based smoothing for triangular, quadrilateral, and quad-dominant meshes. *International Meshing Roundtable.*

Chandar, D. D. J. and M. Damodaran (2009). Computational fluid-structure interaction of a flapping wing in free flight using overlapping grids. *AIAA 2009-3676.*

Codina, R. (2000a). Pressure stability in fractional step element methods for incompressible flows. *Computational Physics 170.*

Codina, R. (2000b). Stabilization of incompressibility and convection trough orthogonal sub-scales in finite element methods. *Computational Physics 190*, 1579–1599.

Combes, S. A. and T. L. Daniel (2005). Flexural stiffness in insect wings. effect of wins venation and stiffness distribution on passive bending. *American entomologist.*

Cook, R., D. S. Malkus, R. J. Witt, and M. E. Plesha (2001). *Concepts and Applications of Finite Element Analysis.* Hardcover.

Degroote, J. (2010). *Development of Algorithms for the Partitioned Simulation of Strongly Coupled Fluid-Structure Interaction Problems.* Ph. D. thesis, Ghent University, Ghent, Belgium.

Dickinson, M. H., F. Lehmann, and S. P. Sane (2004). Wing rotation and the aerodynamic basis of insect flight. *Science 284*, 195460.

Donea, J. and A. Huerta (2003). *Finite Element Methods for Flow Probelms.* John Wiley and Sons.

Guerrero, J. (2008). *Numerical simulation of the unsteady aerodynamics of flapping flight.* Ph. D. thesis, University of Genova, Genova, Italy.

Han, S. M., H. Benaroya, and T. Wei (1999). Dynamics of transversely vibrating beams using four engineering theories. *Journal of Sound and vibration.*

Heathcote, S. and I. Gursul (2005). Flexible flapping airfoil propulsion at low reynolds numbers. *AIAA Paper 2005-1405-CP.*

Kang, C., H. Aono, C. E. S. Cesnik, and W. Shyy (2011). Effects of flexibility on the aerodynamic performance of flapping wings. *6th AIAA Theoretical Fluid Mechanics Conference.*

Kang, C. and W. Shyy (2012). Effects of flexibility on the aerodynamics of a hovering flexible airfoil at reynolds number of 100 to 1000. *AIAA Aerospace Sciences Meeting including the New Horizons Forum and Aerospace Exposition.*

Kassiotis, C., A. Ibrahimbegovic, R. Niekamp, and H. Matthies (2011). Nonlinear fluid-structure interaction problem. part i: implicit partitioned algorithm, nonlinear stability proof and validation examples. *HAL archives-ouvertes.fr.*

Kuttler, U. and W. Wall (2008). Fixed-point fluid-structure interaction solvers with dynamic relaxation. *Computational Mechanics, 43(1):6172.*

Lohner, R. (2001). *Applied CFD Techniques*. John Wiley and Sons.

Maza, M., F. Flores, and S. Preidikman (2012). Interaccion fluido-estructura inestacionaria y no-lineal, con modelos de flujo potencial y estructuras de vigas. *Asociacion Argentina de Mecanica Computacional XXXI*, 771–795.

Naderi, A., M. Mojtahedpoor, and A. Beiki (2016). Numerical investigation of non-stationary parameters on effective phenomena of a pitching airfoil at low reynolds number. *Journal of Applied Fluid Mechanics 9*(2), 643–651.

Olivier, M. (2010). *A Fluid-Structure Interaction Partitioned Algorithm Applied to Flexible Flapping Wing Propulsion*. Ph. D. thesis, Universit Laval, Qubec, Canada.

Pedro, G., A. Suleman, and N. Djilali (2003). A numerical study of the propulsive efficiency of a flapping hydrofoil. *International Journal for numerical methods in fluids 42*, 493526.

Principe, J. and R. Codina (2009). On the stabilization parameter in the subgrid scale approximation of scalar convection-diffusion-reaction equations on distorted meshes. *International Center for Numerical Methods in Engineering*.

Radmanesh, M., O. Nematollahi, M. Nili-Ahmadabadi, and M. Hassanalian (2014). A novel strategy for designing and manufacturing a fixed wing mav for the purpose of increasing maneuverability and stability in longitudinal axis. *Journal of Applied Fluid Mechanics 7*(3), 435–446.

Taylor, G., R. Nudds, and A. Thomas (2003). Flying and swimming animals cruise at a strouhal number tuned for high power efficiency. *Letters to Nature 425*, 707711.

Triantafyllou, G. S., M. S. Triantafyllou, and M. A. Grosenbaugh (1993). Optimal thrust development in oscillating foils with application to fish propulsion. *Fluids and Structures 7*, 205224.

Vazquez, J. G. V. (2007). *Nonlinear Analysis of Orthotropic Membrane and Shell Structures Including Fluid-Structure Interaction*. Ph. D. thesis, Universitat politecnica de catalunya, Barcelona, Spain.

Wall, W. A. and E. Ramm (1998). Fluid-structure interaction based upon a stabilized (ale) finite element method. *IV World Congress on Computational Mechanics, Barcelona*.

Wright, J. R. and J. E. Cooper (2007). *Introduction to aircraft aeroelasticity and loads*. John Wiley and Sons.

Zhu, Q. (2007). Numerical simulation of a flapping foil with chordwise or spanwise flexibility. *AIAA 45*(10), 2448–2457.